Synthesis, Characterization, and Structural and Theoretical Analysis of $Gd_4B_3C_4$: A Novel Rare Earth Metal Borocarbide Containing Two Different Boron−Carbon Arrangements

Christophe Jardin,[†] Oliver Oeckler,[‡] Hansjürgen Mattausch,*[,‡] Arndt Simon,[‡] Jean-François Halet,*[,†] Jean-Yves Saillard,*[,†] and Josef Bauer*[,†]

Laboratoire de Chimie du Solide et Inorganique Moléculaire, UMR CNRS 6511, Institut de Chimie de Rennes, Université de Rennes 1, 35042 Rennes Cedex, France, and Max-Planck-Institut für Festkörperforschung, Heisenbergstrasse 1, 70569 Stuttgart, Germany

Received June 1, 2000

The synthesis by arc-melting techniques, the single-crystal X-ray structure, and the theoretical analysis of $Gd_4B_3C_4$ are reported. It crystallizes in the triclinic space group $P\bar{1}$ with $a = 3.637(2)$ Å, $b = 3.674(2)$ Å, $c = 11.859(5)$ Å, $\alpha = 93.34(5)°$, $\beta = 96.77(5)°$, $\gamma = 90.24(5)°$, and $Z = 1$. In this structure, the boron and carbon atoms form two different types of nonmetal arrangements: 1-D $(BC)_\infty$ branched chains and finite (0-D) linear CBC "molecular" units. $Gd_4B_3C_4$ is the first characterized member of the rare earth metal borocarbide series in which both 1-D and "molecular" 0-D nonmetal atom systems coexist. From the structural and theoretical analysis, the following formal charge distribution can be proposed within the ionic limit: $(Gd^{3+})_4(BC_2^{5-})(BC^{3-})_2.e^-$. Tight-binding calculations suggest that the excess electron in the ionic limit is mainly localized on the Gd atoms (at the bottom of the 5d band), while LAPW calculations favor its localization on the $(BC)_\infty$ chain. The bonding within this compound is fully analyzed and compared to other members of the rare earth metal borocarbide series.

Introduction

The structural chemistry of ternary rare earth metal borocarbide solid-state compounds of general formula $M_xB_yC_z$ (M = Sc, Y, Ln, An) offers a wide diversity of original topologies, especially with respect to the bonding between the nonmetal atoms.[1] From this perspective, they can be classified in three general categories. In the first one, boron and carbon atoms form infinite, planar, two-dimensional (2-D) networks which alternate in the solid with 2-D sheets of metal atoms.[2] In the second category, the nonmetal atoms form infinite one-dimensional (1-D) planar or nearly planar ribbons which are made of zigzag chains of boron atoms to which carbon atoms are attached.[3] These regular or distorted $(BC)_\infty$ branched chains, isolated from each other, are inserted into channels built by the metal atom network. The third category contains compounds in which the nonmetal atoms form linear or quasi-linear finite (0-D) pseudomolecules isolated into cavities formed by the metal atoms.[4] These finite chains can have different sizes ranging from 2 to hitherto 13 nonmetal atoms. In these compounds, chains of different sizes, as well as isolated C atoms, can coexist. The dimensionality of the nonmetal network is related to its electron richness, which can be approximately evaluated through the average valence electron count (VEC) per nonmetal atom, assuming fully oxidized (usually M^{3+}) metal atoms.[1] The lowest VECs (typically between 4.2 and 4.6) are found for the compounds containing 2-D nonmetal networks, while the largest VECs (typically between 5 and 6) are found for the phases containing finite linear nonmetal units. Compounds containing 1-D arrangements of nonmetal atoms have intermediate VEC values, ranging between 5 and 5.4. This trend can be rationalized assuming that formal addition of supplementary electrons to a given compound results in the occupation of B/C antibonding levels, leading to bond breaking and therefore to a lowering of the dimensionality of the nonmetal atom framework. Deep insights into the electronic structure of some of these materials have shown that the metal atoms are not always fully oxidized and that the bonding within the nonmetal atom framework can be understood within a purely ionic $(M_x)^{n+}(B_yC_z)^{n-}$ description in which all of the B and C atoms satisfy the octet rule.[1−4] This ionic approach is very powerful for the rationalization of the structural chemistry of ternary rare earth metal borocarbides. It is however insufficient to account for the metallic behavior of all of these compounds.

So far, no rare earth metal borocarbide containing nonmetal atom subsystems of different dimensionality (2-D, 1-D, or 0-D) has been characterized, with the exception of $Th_3B_2C_3$ in which 1-D $(BC)_\infty$ chains and isolated C atoms are present.[1] In this paper we report the synthesis, crystal, and electronic structures of $Gd_4B_3C_4$, the first characterized rare-earth metal borocarbide in which both 1-D and polyatomic 0-D nonmetal atom systems are coexisting.

Experimental Section

Synthesis. Mixtures of powders of commercially available elements of high purity (99.99% gadolinium ingots: Rhône Poulenc, Arizona; 99.8% crystalline boron powder, H. C. Starck,

[†] Université de Rennes.
[‡] Max-Planck-Institut für Festkörperforschung.

(1) Bauer, J.; Halet, J.-F.; Saillard, J.-Y. *Coord. Chem. Rev.* **1998**, *178−180*, 723 and references therein.
(2) (a) Wiitkar, F.; Halet, J.-F.; Saillard, J.-Y.; Rogl, P.; Bauer, J. *Inorg. Chem*. **1994**, *33*, 1297. (b) Wiitkar, F.; Kahlal, S.; Halet, J.-F.; Saillard, J.-Y.; Bauer, J.; Rogl, P. *J. Am. Chem. Soc.* **1994**, *116*, 251.
(3) Wiitkar, F.; Kahlal, S.; Halet, J.-F., Saillard, J.-Y.; Bauer, J.; Rogl, P. *Inorg. Chem*. **1995**, *34*, 1248.
(4) (a) Halet, J.-F.; Saillard, J.-Y.; Bauer, J. *J. Less-Common Met*. **1990**, *158*, 239. (b) Ansel, D.; Bauer, J.; Bonhomme, G.; Boucekkine, G.; Frapper, G.; Gougeon, P.; Halet, J.-F.; Saillard, J.-Y.; Zouchoune, B. *Angew. Chem., Int. Ed. Engl*. **1996**, *35*, 2098. (c) Bauer, J.; Boucekkine, G.; Frapper, G.; Halet, J.-F.; Saillard, J.-Y.; Zouchoune, B. *J. Solid State Chem.* **1997**, *133*, 190. (d) Bidaud, E.; Hiebl, K.; Hoffmann, R.-D.; Pöltgen, R.; Jardin, C.; Bauer, J.; Gautier, R.; Gougeon, P.; Saillard, J.-Y.; Halet, J.-F. *J. Solid State Chem.* **2000**, *154*, 286.

10.1021/ic000585y CCC: $19.00
Published on Web 11/30/2000

Table 1. Crystallographic Data for $Gd_4B_3C_4$

fw	354.74	
cryst syst	triclinic	
space group, Z	$P\bar{1}$, 1	
lattice parameters	$a = 3.637(2)$ Å	$\alpha = 93.34(5)°$
	$b = 3.674(2)$ Å	$\beta = 96.77(5)°$
	$c = 11.859(5)$ Å	$\gamma = 90.24(5)°$
vol (Å^3)	157.0(1)	
temp (K)	293	
calcd density (g/cm^3)	7.51	
abs coeff (mm^{-1})	41.53	
R1, wR2 ($>2\sigma$)[a]	0.040, 0.107	

[a] $R1 = \Sigma||F_o| - |F_c||/\Sigma|F_o|$. $wR2 = \{\Sigma[w(F_o^2 - F_c^2)^2]/[w(F_o^2)^2]\}^{1/2}$, where $w = 1/[\sigma^2(F_o^2) + (0.028P)^2 + 24.13P]$ with $P = \mathrm{Max}(F_o^2) + (2F_c^2)/3$.

Germany; 99.98% graphite powder, Carbone-Lorraine, France) were compacted in stainless steel dies without the use of binders or lubricants. The pellets were arc-melted under purified (Ti-gettered) argon with a thoriated tungsten electrode. The alloy buttons were turned over and remelted three times to ensure their homogeneity. Weight losses were checked to be within 1% of the original mass (1 g). The molten pellets were broken into two parts. One part was studied in as-cast condition; the second part was annealed at 1000 °C in silica tubes under primary vacuum for 10 days and subsequently quenched in water at room temperature. To avoid any contamination, the samples were wrapped in molybdenum foils. The pellets had to be kept in sealed silica tubes under primary vacuum to prevent hydrolysis of the samples.

X-ray Diffraction. Powder samples were characterized by a modified Guinier technique[6] (detection with imaging plates, Fuji BAS5000) using capillaries sealed under dried Ar to avoid hydrolysis. The samples appear to be single-phase, but diffraction patterns are rather diffuse. For the determination of lattice constants only 20 reflections could be used. The refined values of the triclinic cell are $a = 3.635(2)$ Å, $b = 3.672(2)$ Å, $c = 11.844(6)$ Å, $\alpha = 93.31(5)°$, $\beta = 96.70(5)°$, $\gamma = 90.33(5)°$. Lamina-shaped crystals were checked for their quality by Buerger precession exposures. A data set was collected on a Stoe IPDS one-circle diffractometer with an imaging plate area detector using graphite monochromated Mo Kα radiation. A numerical absorption correction (Gaussian integration) based on six indexed and measured faces was applied.[7] Some important crystallographic data are given in Table 1. The structure could be solved using the Patterson method.[8] The refinement[9] converged well, and the carbon and boron atoms could be located from difference Fourier maps. Only the Gd atoms were refined anisotropically. The displacement parameter of the B(2) atom is significantly larger than those of the other atoms, but this may be explained as due to the rather long B−B bonds. Local deviations from the averaged structure cannot be excluded. The refined atomic coordinates and selected interatomic distances are given in Tables 2 and 3, respectively. The positions of the light atoms are less well defined than those of the Gd atoms. Single-crystal lattice parameters were determined with an Enraf Nonius CAD4 four-circle diffractometer. The refined lattice parameters (see Table 1) from 25 centered high-order reflections were considered to be more reliable than the powder data and have been used for the calculation of interatomic distances and angles.

Table 2. Positional and (Equivalent) Isotropic Displacement Parameters for $Gd_4B_3C_4$

atom	x	y	z	U_{eq}/U_{iso} (Å^2)[a]
Gd(1)	0.1980(3)	0.9717(3)	0.34983(7)	0.0063(3)
Gd(2)	0.6124(2)	0.4354(2)	0.13729(7)	0.0052(3)
C(1)	0.123(6)	0.927(6)	0.1202(17)	0.008(4)
C(2)	0.697(5)	0.464(5)	0.3317(16)	0.007(3)
B(1)	0	0	0	0.010(6)
B(2)	0.740(13)	0.477(13)	0.455(4)	0.045(9)

[a] U_{eq} is defined as one-third of the trace of the orthogonalized $\mathbf{U}_{ij}$ tensor. B and C atoms have been refined isotropically.

Table 3. Selected Interatomic Distances (Å) for $Gd_4B_3C_4$

Gd(1)−Gd(1)	3.637(2)	C(1)−Gd(1)	2.70(2)	B(1)−Gd(2)	2.729(2)
Gd(1)−Gd(1)	3.674(2)	C(1)−Gd(2)	2.54(2)	B(1)−Gd(2)	2.997(2)
Gd(1)−Gd(1)	3.950(2)	C(1)−Gd(2)	2.56(2)	B(2)−Gd(1)	2.83(4)
Gd(1)−Gd(1)	3.990(2)	C(1)−Gd(2)	2.62(2)	B(2)−Gd(1)	2.83(5)
Gd(1)−Gd(2)	3.583(2)	C(1)−Gd(2)	2.66(2)	B(2)−Gd(1)	2.89(4)
Gd(1)−Gd(2)	3.589(3)	C(2)−Gd(1)	2.57(2)	B(2)−Gd(1)	2.90(4)
Gd(1)−Gd(2)	3.590(2)	C(2)−Gd(1)	2.58(2)	B(2)−Gd(1)	2.91(5)
Gd(1)−Gd(2)	3.612(3)	C(2)−Gd(1)	2.59(2)	B(2)−Gd(1)	2.97(4)
Gd(2)−Gd(2)	3.637(2)	C(2)−Gd(1)	2.62(2)	C(1)−B(1)	1.48(2)
Gd(2)−Gd(2)	3.674(2)	C(2)−Gd(2)	2.28(2)	C(2)−B(2)	1.45(5)
Gd(2)−Gd(2)	3.322(2)			B(2)−B(2)	2.06(9)
				B(2)−B(2)	2.15(10)

Electronic Band Structure Calculations. Extended Hückel tight-binding[10] calculations were carried out on the crystal stucture of $Gd_4B_3C_4$ using the program YAeHMOP.[11] The exponents (ζ) and valence shell ionization potentials (H_{ii} in eV) were, respectively: 1.3, −15.2 for B 2s; 1.3, −8.5 for B 2p; 1.625, −21.4 for C 2s; 1.625, −11.4 for C 2p; 2.14, −7.24 for Gd 6s; and 2.08, −4.65 for Gd 6p. The H_{ii} value for Gd 5d was at −8.08. A linear combination of two Slater-type orbitals with exponents $\zeta_1 = 3.78$ and $\zeta_2 = 1.38$ with the weighting coefficients $c_1 = 0.7765$ and $c_2 = 0.4586$ was used to represent the Gd 5d atomic orbitals.

Density functional calculations were also performed on the crystal structure of $Gd_4B_3C_4$ using the full-potential linearized augmented plane wave (LAPW) method implemented in the WIEN97 program.[12] The local density approximation of Perdew and co-workers[13] was used within the generalized gradient approximation of Perdew, Burke, and Erzerhof.[14] In this method the cell is partitioned into spheres centered at the nuclear positions (muffin-tin radii in a.u., 2.3 for Gd and 1.37 for B and C) and an interstitial region where Bloch wave functions are expanded in plane waves. Within the spheres these plane waves are augmented by atomic-like functions. The valence states were treated scalar-relativistically. For "semi-core states" the LAPW basis set was extended by local orbitals. The core states were treated relativistically including spin−orbit coupling. Gd being a ferromagnet, spin-polarized calculations in which 4f orbitals treated as band states were performed.

Results and Discussion

Crystal Structure. Although the structure of $Gd_4B_3C_4$ is triclinic, the environments of the boron−carbon substructures

(5) Rogl, P. *J. Nucl. Mater.* **1979**, *79*, 154.
(6) Simon, A. *J. Appl. Crystallogr.* **1970**, *3*, 11.
(7) *XPREP − Data Preparation & Reciprocal Space Exploration*, ver. 5.1/NT; Brücker Analytical X-ray Systems, 1997.
(8) Sheldrick, G. M. *SHELX/S, Program for the Solution of Crystal Structures*; Universität Göttingen: Göttingen, 1997.
(9) Sheldrick, G. M. *SHELX/L, Program for the Refinement of Crystal Structures*; Universität Göttingen: Göttingen, 1997.
(10) (a) Hoffmann, R. *J. Chem. Phys.* **1963**, *39*, 1397. (b) Whangbo, M.-H.; Hoffmann, R. *J. Am. Chem. Soc.* **1968**, *100*, 6093.
(11) Landrum, G. A. *YAeHMOP − Yet Another extended Hückel Molecular Orbital Package*, release 2.0; Ithaca, NY, 1997.
(12) Blaha, P.; Schwarz, K.; Luitz, J. *WIEN97*, Vienna University of Technology, 1997. Improved and updated Unix version of the original copyrighted WIEN-code (Blaha, P.; Schwarz, K.; Sorantin, P.; Trickey S. B. *Comput. Phys. Commun.* **1990**, *59*, 1990).
(13) Perdew, J. P.; Chevary, J. A.; Vosko, S. H.; Jackson, K. A.; Pederson, M. R.; Singh, D. J.; Fiolhais, C. *Phys. Rev.* **1992**, *B46*, 6671.
(14) Perdew, J. P.; Burke, K.; Ernzerhof, M. *Phys. Rev. Lett.* **1996**, *77*, 7865.

Scheme 1

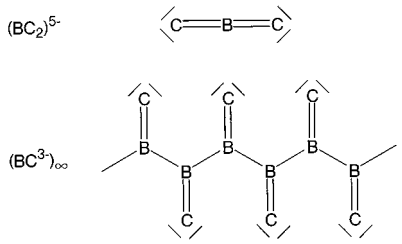

have rather high local symmetry. The crystal contains finite (0-D) CBC units, as well as 1-D $(BC)_\infty$ chains. The C(1) and B(1) atoms form linear CBC units with short B−C separations of 1.48(2) Å, indicative of double bonds. Therefore, the formal charge of 5− can be assigned to these triatomic units, rendering them isoelectronic to CO_2, as schematized in Scheme 1. Similar $(CBC)^{5-}$ entities have been shown to exist in other metal boride carbide compounds[1] such as Al_3BC_3[15] and Sc_2BC_2[4a] where the B−C distances are 1.44 and 1.48 Å, respectively. Linear isoelectronic anions such as (C_3),$^{4-}$ $(CBN)^{4-}$, or $(NBN)^{2-}$ have also been shown to exist in the solid state.[16]

As in many rare earth boride carbides[1] and boride carbide halides[17] the C(1) atoms are located in a (slightly distorted) square pyramidal environment of metal atoms. As a result, the B(1) atoms lie in the middle of elongated cubes of Gd atoms.

The $(BC)_\infty$ ribbons are almost perfectly planar. Their zigzag boron chain exhibits a slight bond alternation with two crystallographically different B(2)−B(2) distances of 2.06(9) Å and 2.15(10) Å. Owing to the associated standard deviations, these distances are not significantly different and the zigzag chains can be considered as regular, as observed in YBC[18] or UBC[19] where the B−B distances are 2.00 and 1.90 Å, respectively, in contrast to ThBC in which a strong B−B bond alternation is observed (1.77 and 2.47 Å).[20] Similar $(BC)_\infty$ regular chains have been shown to exist in Ce_3Br_3BC[17] and $Gd_4Br_3BC_2$[21] with B−B distances of 2.18 and 2.08 Å, respectively. The B(2)−C(2) distance of 1.45(5) Å is indicative of a double bond. With two BBC bond angles of 120.1° and 119.9° and the BBB angle of 119.4°, the B(2) atom is almost perfectly sp^2-hybridized. Calculations have shown that the formal charge of 3− per BC repeat unit can be assigned to this type of regular arrangement in which all the atoms obey the octet rule, as shown in Scheme 1.[1,3]

The C(2) atoms of the $(BC)_\infty$ chains in $Gd_4B_3C_4$ are also found in square pyramids which cap distorted trigonal prisms centered by boron atoms. The Gd_6B prisms are fused via the triangular and the two uncapped rectangular faces to form layers. These layers are connected by a layer of distorted cubes centered by the boron atoms of the CBC units (see Figure 1).

Thus, from the crystal structure analysis, the following formal charge distribution can be proposed within the ionic limit: $(Gd^{3+})_4(BC_2^{5-})(BC^{3-})_2.e^-$. One can suggest that, as in Sc_2BC_2, formally $(Sc^{3+})_2(BC_2^{5-}).e^-$,[4a] the excess electron in the ionic limit lies in the metal d-band, i.e., the metal atoms are not fully oxidized. A deeper insight of the electronic structure of $Gd_4B_3C_4$ is given below.

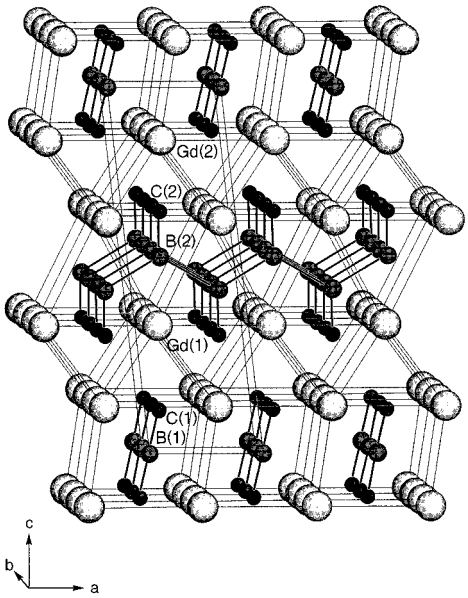

Figure 1. Crystal structure of $Gd_4B_3C_4$.

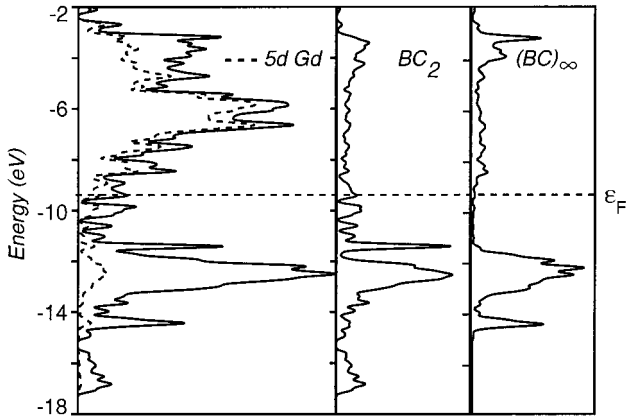

Figure 2. Extended Hückel tight-binding total DOS (left side in solid line) and its projections on the 5d Gd orbitals, the BC_2 units, and the $(BC)_\infty$ chains.

Extended Hückel Tight-Binding Analysis. The total density of states (DOS) of $Gd_4B_3C_4$ is shown in Figure 2, together with the projections on the Gd 5d orbital, the CBC units and the $(BC)_\infty$ chains. The states constituting the large band situated above the Fermi level are of dominant Gd 5d character, in agreement with almost fully oxidized metal. Except for the small band lying right below the Fermi level which is equally localized on the metal and nonmetal atoms, all occupied levels have a dominant nonmetal atom character. Figure 3 shows the frontier orbitals of an isolated $(CBC)^{5-}$ unit and their projection in the DOS of $Gd_4B_3C_4$. Their electron occupations in the crystal are given in parentheses. They clearly confirm the 5− formal charge of the CBC units. However, a significant electron donation from the occupied frontier orbitals of the $(CBC)^{5-}$ (including the bonding π_u ones) into the vacant 5d metal AOs is computed. The small occupation of the antibonding π_u* levels is indicative of a very weak back-donation. This is at variance with Sc_2BC_2 in which the π_u* occupation was computed to be 0.229.[4a] Obviously, even with a high oxidation state and unlike a lanthanoid atom, a transition metal has still some electron back-donation ability. The B−C overlap population in an isolated

(15) Hillebrecht, H.; Meyer, F. D. *Angew. Chem., Int. Ed. Engl.* **1996**, *35*, 2499.
(16) (a) Pöttgen, R.; Jeitschko, W. *Inorg. Chem.* **1991**, *30*, 427. (b) Meyer, H.-J.; Hoffmann, R. *Z. Anorg. Chem.* **1992**, *607*, 57 and references therein. (c) Mattausch, Hj.; Gulden, T.; Kremer, R. K.; Horakh, J.; Simon, A. *Z. Naturforsch.* **1994**, *496*, 1439.
(17) Mattausch, Hj.; Oeckler, O.; Simon, A. *Inorg. Chim. Acta* **1999**, *289*, 174.
(18) (a) Bauer, J.; Nowotny, H. *Monatsh. Chem.* **1971**, *102*, 1129. (b) Bauer, J. *J. Less-Common Met.* **1982**, *87*, 45.
(19) Toth, L.; Nowotny, H.; Benesovsky, F.; Rudy, E. *Monatsh. Chem.* **1961**, *92*, 794.
(20) Rogl, P. *J. Nucl. Mater.* **1978**, *73*, 198.

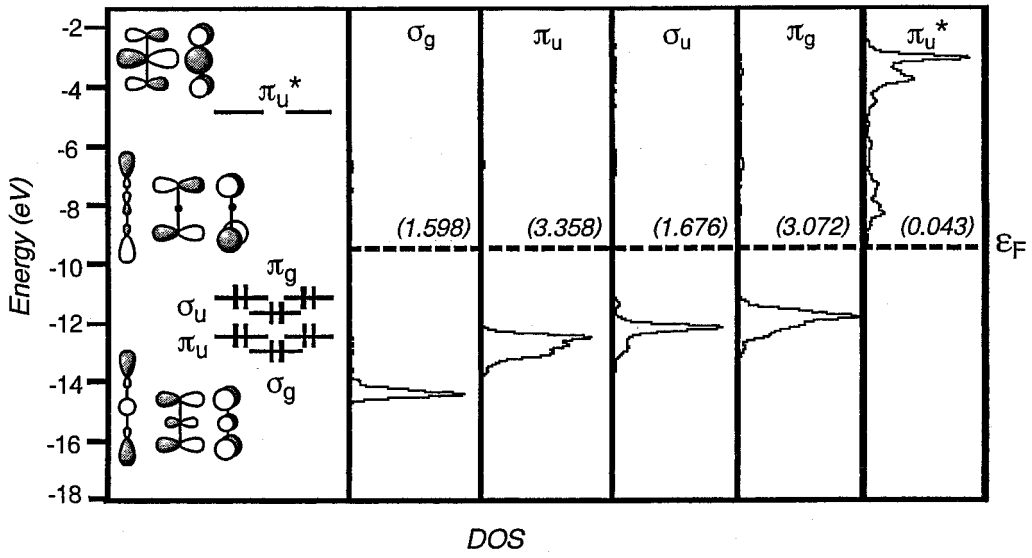

Figure 3. The frontier orbitals of an isolated $(BC_2)^{5-}$ unit (left), and their projections on the DOS of $Gd_4B_3C_4$ (extended Hückel tight-binding calculations). Their electron occupation is given in brackets.

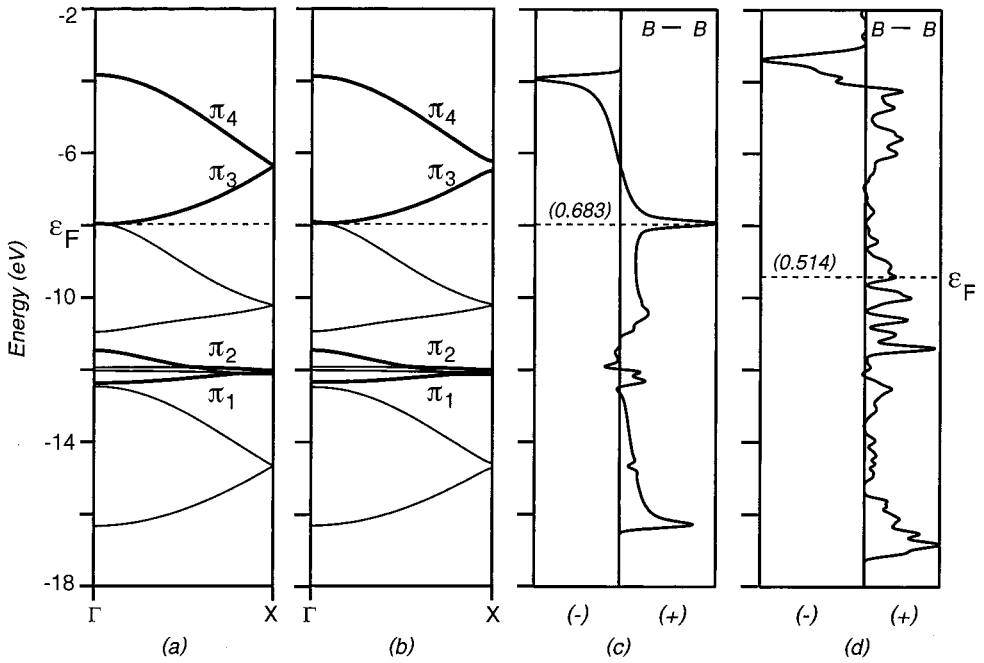

Figure 4. (a) Band structure for an isolated 1-D regular $(BC)_\infty$ chain, assuming averaged metrical data taken from $Gd_4B_3C_4$. (b) Band structure for an isolated 1-D $(BC)_\infty$ chain taken from the crystal structure of $Gd_4B_3C_4$. (c) B−B COOP curve computed for an isolated 1-D $(BC)_\infty$ chain taken from the crystal structure of $Gd_4B_3C_4$. (d) B−B COOP computed for $Gd_4B_3C_4$ (extended Hückel tight-binding calculations; π-bands are in bold; values in parentheses are the computed B−B overlap populations).

$(CBC)^{5-}$ anion is 1.274. It drops to 1.151 in $Gd_4B_3C_4$, a consequence of the donation of π-bonding electrons to the metal ions.

Although the B−B bond alternation is not significant from the experimental structural point of view, we have estimated its influence on the bonding within the $(BC)_\infty$ chains, first by carrying out calculations on an isolated 1-D $(BC^{3-})_\infty$ polymer, considering both the regular averaged and the experimentally observed structures. The corresponding band structures are shown in Figure 4a,b. The band structure of the regular model is not significantly different from that calculated previously with slightly different bond lengths.[3] One should note the accidental near-degeneracy at Γ of the highest occupied band, which is of σ-type and weakly antibonding at Γ,[3] and the lowest unoccupied band, which is of π-type. When the bond alternation is applied the loss of the screw axis induces a degeneracy splitting at X. However, all of the gaps which are opened at X are found to be negligible (Figure 4b). This result suggests that the small bond alternation observed in the $(BC)_\infty$ chains cannot be considered as the result of a significant first-order Peierls distortion but rather from a slightly different environment in $Gd_4B_3C_4$ of the two crystallographically different B−B bonds. This bond alternation does neither change the near σ/π degeneracy observed at Γ nor it opens a gap at the Fermi level. The computed B−B overlap populations in one isolated $(BC^{3-})_\infty$ chain are 0.710 and 0.655 for the distances of 2.06 and 2.15 Å, respectively. In $Gd_4B_3C_4$ these values are reduced to 0.547 and 0.481, respectively, as the result of the donation of both σ- and π-bonding electrons to the metal cations. This is exemplified by Figure 4b,c which shows the average B−B COOP curves computed for the isolated $(BC^{3-})_\infty$ chain and for the real $Gd_4B_3C_4$ compound.

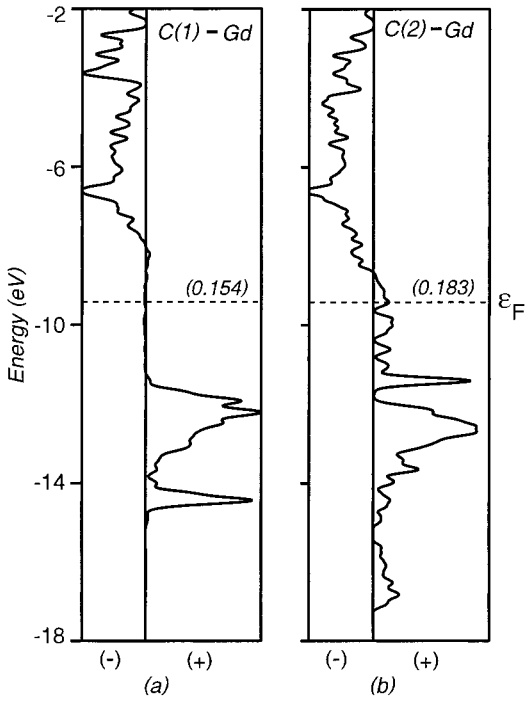

Figure 5. Extended Hückel tight-binding averaged Gd−C COOP curves. Values in parentheses are the computed Gd−C overlap populations.

COOP curves represent the variation of interatomic overlap populations with respect to energy.[22] They are indicative of the strength of a bonding/antibonding interaction at a given energy. In $Gd_4B_3C_4$ there are more unoccupied B−B bonding states than in an isolated $(BC^{3-})_\infty$ chain (compare Figure 4c,d). The B−C overlap population is also reduced, but to a lesser extent, when going from the isolated 1-D chain to the real 3-D compound (1.162 vs 1.100), as the result of some B−C π-bonding donation to the metal atoms. The latter value compares well with that computed for the B−C bonds of the (CBC) units in $Gd_4B_3C_4$ (1.151).

Figure 5 shows the Gd−C COOP curves for C(1) and C(2) averaged over their five Gd nearest neighbors. They show clearly that almost all the Gd−C bonding states are occupied whereas the corresponding antibonding states are vacant. Thus, the electron count of $Gd_4B_3C_4$ nearly maximizes the metal−carbon bonding. The corresponding averaged overlap populations are reported in Figure 5. They are indicative of significant (although not very large) covalent interactions. The Gd−B COOP curves (not shown here) exhibit similar shapes, but the bonding interactions are much weaker as indicated by the Gd−B(1) and Gd−B(2) average overlap populations which are 0.018 and 0.041, respectively. These Gd−B and Gd−C interactions result in some significant nonmetal-to-metal electron donation, as exemplified by the following computed net charges $[Gd(1)^{1.37+}]_2$ $[Gd(2)^{1.42+}]_2$ $(BC_2)^{2.59-}$ $[(BC)^{1.50-}]_2$. As expected, they are significantly different from the formal charges (or group oxidation states) proposed above and based on a purely ionic scheme of bonding between the metal cations and the anionic nonmetallic framework.

DFT-LAPW Analysis. Although the tight-binding calculations described above allow detailed orbital and fragment orbital analysis of $Gd_4B_3C_4$, they provide results only at a qualitative level. Moreover, the Gd 4f orbitals were not included in the calculations. To obtain a more quantitative overview of the electronic structure of the title compound, spin-polarized LAPW calculations were also carried out. The total and various projected LAPW DOS are shown in Figure 6. The main difference with the tight-binding DOS is the presence of the 4f states which form rather narrow (nonbonding) bands. Since there are two crystallographically different Gd atoms, they give rise to slighly shifted 4f peaks which are overlapping. There are two overlapping occupied 4f peaks (spin down) and two overlapping unoccupied 4f peaks (spin up). This nonequivalence of the Gd atoms is the main reason for the fact that the 4f peaks are not very narrow. The spin-up (occupied) and spin-down (vacant) 4f states are separated by ca. 5 eV. The metal 4f and 5d projections indicate some weak hybridization. The LAPW 5d projection exhibits a larger dispersion than the tight-binding projection (compare Figure 6 with Figure 2). There are also proportionally less occupied 5d states in the LAPW projection, suggesting a higher oxidation state. In addition, the LAPW total and projected DOS are in a qualitative agreement with those obtained from the tight-binding calculations. The integration of the electron density inside the gadolinium muffin-tin spheres leads to almost exactly a 3+ charge. Assuming that the 26.6 electrons which lie in the intersphere region are mostly valence electrons to be shared by all the unit cell atoms leads to suggest a higher ionic character of $Gd_4B_3C_4$, as compared to the tight-binding results.

Conclusion

$Gd_4B_3C_4$ is the first characterized member of the rare earth metal borocarbide series in which both 1-D and "molecular" 0-D nonmetal atom systems are coexisting. Assuming complete oxidation of the metals, the average VEC per nonmetal atom is 5.3. This value falls in a region where the VEC ranges of compounds having only 1-D and compounds having only 0-D nonmetal atom systems are overlapping.[1] The structural and tight-binding analyses suggest the group oxidation states for the anions, BC_2^{5-} and BC^{3-}, respectively, i.e., the metal atoms are not fully oxidized. The LAPW results tend to favor full metal oxidation, which could correspond to different group oxidation states, BC_2^{5-} and BC,$^{3,5-}$ respectively.[23] It is interesting to note that in this particular situation, the excess electron in the ionic limit (vide supra) is not metal atom centered but is delocalized in the 1-D $(BC)_\infty$ chain, which reminds the bonding situation of alkali metal-doped polyacetylene.[24] It would correspond to the occupation of the bottom-half of the π_3 band in Figure 4b and could be interpreted as being the cause of the slight B−B bond alternation observed in $Gd_4B_3C_4$. This would render almost equal the average atomic VEC of the $(BC_2)^{5-}$ units and the $(BC^{3.5-})_\infty$ chains ($\sim$5.3). Nevertheless, these small differences in group oxidation states suggested by both types of calculations are likely not to be significant, owing to the existence of supplementary charge-transfer accompanying the metal-to-nonmetal covalent bonding which is shown to be significant in $Gd_4B_3C_4$ as in most of the rare earth metal borocarbide compounds.[1]

(21) Mattausch, Hj.; Simon, A. *Angew. Chem., Int. Ed. Engl.* **1995**, *34*, 1633.
(22) Hoffmann, R. *Solid and Surfaces. A Chemist's View of Bonding in Extended Structures*; VCH: Weinheim, 1988.
(23) One referee suggested the possibility for the excess electron to be housed in the CBC units. This would require the occupation of the π^*_u MOs (Figure 3) which are too high in energy in the CBC linear arrangement, as shown by the calculations. It is likely that the partial occupation of the π^*_u MOs would force these units to bend.
(24) Burdett, J. K. *Chemical Bonding in Solids.* Oxford University Press: Oxford, 1995.

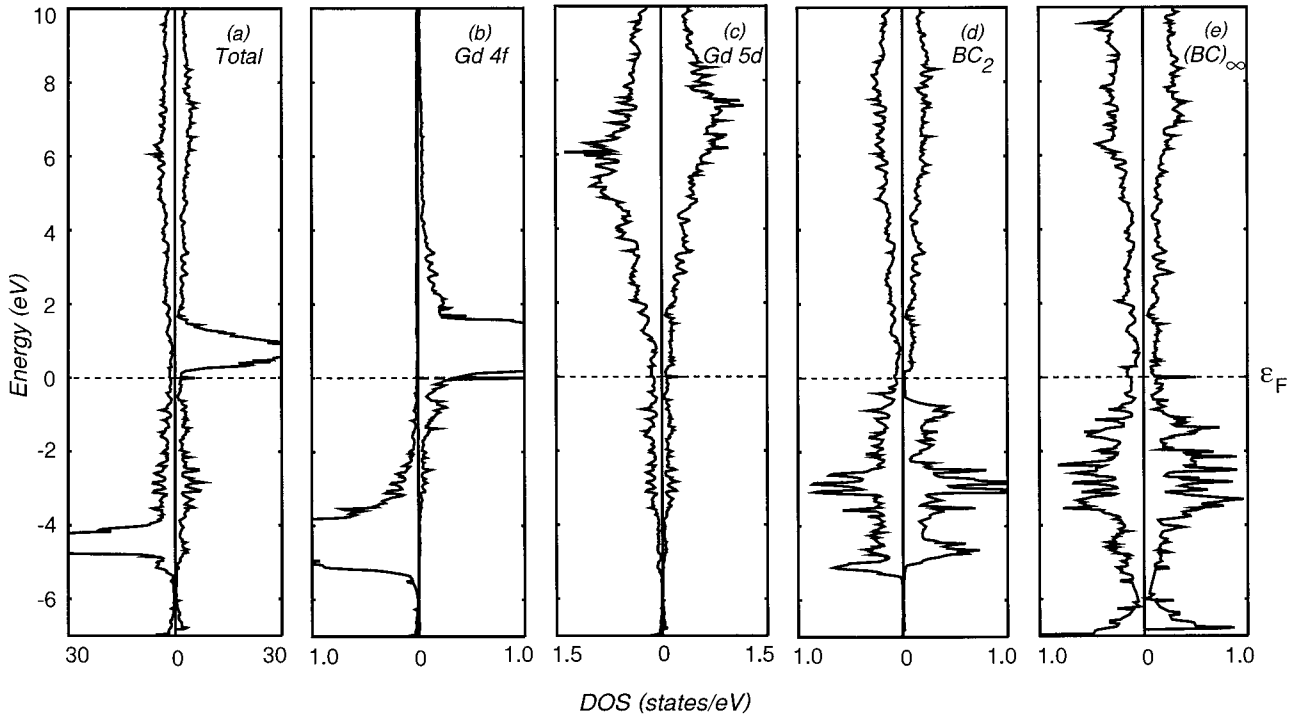

Figure 6. LAPW total DOS and its projections on the 4f and 5d Gd orbitals, on the BC_2 units and on the $(BC)_\infty$ chains (spin-polarized calculations).

Acknowledgment. All band structure calculations were carried out at the computing centers IDRIS-CNRS (Orsay) and CRI (Rennes).

Supporting Information Available: Figure showing the crystal structure with the thermal vibrational (50%) ellipsoids of the Gd atoms. One X-ray crystallographic file, in CIF format. This material is available free of charge via the Internet at http://pubs.acs.org.

IC000585Y